Boundary slip dependency on surface stiffness

Nikolaos Asproulis and Dimitris Drikakis*

Fluid Mechanics & Computational Science Group, Department of Aerospace Sciences, Cranfield University, Cranfield, Bedfordshire MK43 0AL, United Kingdom

(Received 12 September 2009; revised manuscript received 13 April 2010; published 24 June 2010)

The paper investigates the effects of surface stiffness on the slip process aiming to obtain a better insight of the momentum transfer at nanoscale. The surface stiffness is modeled through the stiffness, κ, of spring potentials, which are employed to construct the thermal walls. It is shown that variations of stiffness, κ, influence the slip mechanism either toward slip or stick conditions. Increasing the values of κ alters the oscillation frequency and the mean displacement of the wall particles toward higher and lower values, respectively. Our results suggest that the amount of slip produced as a function of stiffness follows a common pattern that can be modeled through a fifth-order polynomial function.

DOI: 10.1103/PhysRevE.81.061503 PACS number(s): 83.50.Rp, 68.08.−p, 68.35.Ct, 83.10.Rs

I. INTRODUCTION

During the past decade micro and nanofluidics have emerged as vital tools in the development of nanoscale analysis and manufacturing systems. As the devices operational dimensions are downsized to micro- and nanoscales the surface-to-volume ratio increases and the interfacial interactions dominate the flow phenomena. The effects of surface interactions are macroscopically formulated via appropriate boundary conditions. In the majority of the macroscale flows the fluid is considered to be immobile near the solid boundary; however, as the scales shrink a number of experimental studies [1–3] revealed the presence of slippage. In these cases, where the continuum no-slip approximation breaks down, the slip's magnitude is quantified through the slip length ($L_s = \frac{u_{slip}}{\partial u/\partial n}$), which represents the extrapolated distance from the wall to the point with zero tangential velocity component. Surface structure, wettability and, nanoscale roughness are some of the factors that have been recognized to affect slippage phenomena [4,5]. Generally, the parameters that contribute to slip generation along with their implications to the slip's magnitude, are not explicitly known and fully understood [6]. Therefore, identifying and quantifying their impact poses a great challenge that needs to be better understood in order to assist with the development of micro and nanofluidic devices.

High-fidelity computational modeling has been employed to compliment experiments relating to slippage effects, primarily due to accuracy issues relating to instrumentation used for measuring physical quantities at nanoscale. Molecular dynamics [7–10] (MD) simulations have been employed to study the slip mechanism and shed light on the effects of parameters such as nanoroughness and surface wettability on the slip's magnitude.

It is commonly recognized [6] that surface corrugation can greatly influence the interfacial flow characteristics. However, it is still unclear whether it contributes toward slip or stick conditions, since experimental evidence [3,11,12] suggests that both possibilities exist. Despite a number of numerical studies [13,14], the slip rate as a factor of roughness has not been fully quantified. An important factor in the slip process, which may elucidate the variability of the experimental and numerical outcomes, is surface stiffness. In the current study, MD simulations are employed to study the slip length's dependency on the wall stiffness for a Lennard-Jones (LJ) fluid.

II. SIMULATION METHOD

The computational domain consists of monoatomic fluid particles confined by two stationary thermal walls separated by a distance L_y along the y direction. The size of the computational domain is $L_x = 16.97\sigma$, $L_y = 34.64\sigma$, and $L_z = 6.53\sigma$, where σ is the molecular length scale; periodic boundary conditions are applied in the parallel to the walls directions x and z. The interatomic interactions among the fluid molecules are modeled through a LJ potential, which for a pair of molecules i,j with distance r_{ij} is

$$\nu_{ij}^{LJ}(r_{ij}) = 4\epsilon[(\sigma/r_{ij})^{12} - (\sigma/r_{ij})^{6}], \tag{1}$$

where ϵ is the characteristic energy level. All the interatomic interactions are truncated at a cutoff distance $r_c = 2.2\sigma$. The fluid density is selected to be $\rho_{fluid} = 0.81\ m\sigma^{-3}$, where m is the mass of a fluid molecule, and corresponds to the generation of 2880 particles. A constant external force f_x along the x direction is applied to each fluid molecule to drive the flow. The simulations have been performed for a range of force values spanning from $f_x = 0.005\ \epsilon\sigma^{-1}$ to $f_x = 0.015\ \epsilon\sigma^{-1}$ with step $0.0025\ \epsilon\sigma^{-1}$. The velocity profile from a continuum hydrodynamics perspective, assuming a slip velocity u_{slip} at the solid boundary, is

$$u_x(y) = 0.5\mu^{-1}\rho f_x[(L_y/2)^2 - y^2] + u_{slip} \tag{2}$$

The parabolic velocity profile [Eq. (2)] implies that the shear rate is proportional to the applied force and, consequently, the force variations correspond to subsequent adjustments of the shear rate. Previous computational studies [7,9,15] have indicated a non linear relationship between the shear rate and the slip length. Therefore, aiming to minimize the influence of the shear rate, the effects of the wall stiffness on slip

*d.drikakis@cranfield.ac.uk

phenomena is studied for a broad range of shear rates. The magnitude of the applied force should be carefully selected since high force values can drive the system out of the linear response regime [16]. The excessive viscous heating of the system is dissipated through a Langevin thermostat [7], applied only in the z direction to circumvent any influence in the flow direction. The equations of motion along the z direction are

$$m\ddot{z}_i + m\Gamma\dot{z}_i = -\sum_{i\neq j}\frac{\partial V_{ij}}{\partial z_i} + \eta_i, \tag{3}$$

where η_i is a Gaussian distributed random force with zero mean $\langle \eta_i(t)\rangle = 0$ and variance $\langle \eta_i(0)\eta_j(t)\rangle = 2mk_BT\Gamma\delta(t)\delta_{ij}$, and $T = 1.1\ \epsilon k_B^{-1}$ is the fluid temperature. The friction coefficient has been selected to be $\Gamma = 1.0\ \tau^{-1}$ throughout the simulations, aiming to minimize undesirable effects on the self-diffusion coefficient [9,17]. The equations of motion are integrated using a velocity-Verlet algorithm [18] with time step $\delta t = 0.001\tau$; 6×10^5 time steps have been performed for equilibration and another 6×10^5 time steps for averaging.

Each of the solid walls is modeled as two (111) fcc lattice planes with density $\rho_{wall} = 4.0\ m\sigma^{-3}$ corresponding to 528 particles with mass equal to the fluid ones. The wall particles interact with the fluid through a LJ potential with energy and length scales ϵ_{wf} and σ_{wf}, respectively. Generally, slippage phenomena are sensitive to the wall-fluid interactions, particularly, as the wall (surface) energy decreases, the amount of momentum transferred across the interface decreases, thus leading to larger slip values [7]. Therefore, the effects of surface stiffness are studied for two sets of interfacial parameters (i) $\epsilon_{wf} = 0.2\epsilon$, $\sigma_{wf} = 0.75\sigma$ and (ii) $\epsilon_{wf} = 0.4\epsilon$, $\sigma_{wf} = 0.75\sigma$. Every wall particle i is attached to its equilibrium lattice site $\boldsymbol{r}_0$ with an elastic spring force

$$\boldsymbol{F} = -\kappa(\boldsymbol{r}_i - \boldsymbol{r}_0), \tag{4}$$

where κ is the wall stiffness. Stiffness is a pivotal parameter that provides a link between the wall model and real materials and determines the physical properties at the wall. Its values reveal the strength of particles bonds and larger rates are related to higher melting points and Young's modulus. Their selection should not allow (i) the mean square displacement of the wall atoms to be larger than the Lidemann criterion of melting [9,19] and (ii) the movement of the wall atoms to be in a regime that cannot be entirely addressed in the molecular simulation time step [9]. For the current study, κ, ranges from $\kappa = 100\ \epsilon\sigma^{-2}$ to $\kappa = 1200\ \epsilon\sigma^{-2}$; this interval is consistent with typical κ magnitudes employed in previous MD studies [9,20,21]. Although it is not straight forward to establish exact relations between simplified models such as the one employed here for the wall, and real physical substances, the selected values of solid stiffness correspond to a broad range of real materials, including silicon based structures, that are primarily used for microfluidic fabrications and, typically, their Young modulus is lower compared to the metals one [22]. The wall temperature is kept constant, $T_{wall} = 1.1\ \epsilon k_B^{-1}$ during the simulations through a velocity rescaling thermostat [23].

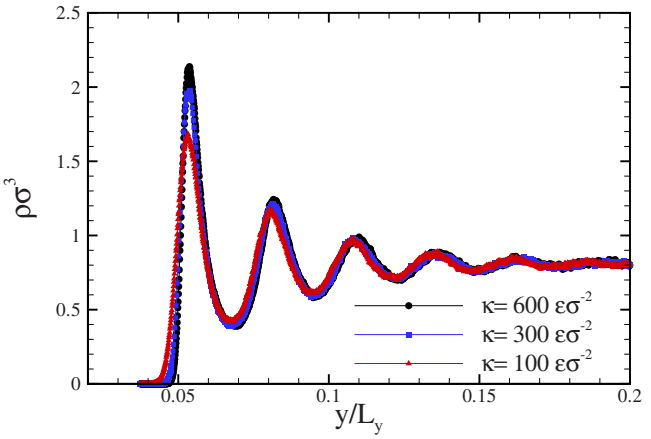

FIG. 1. (Color online) Density profiles near the lower wall for various values of the spring stiffness κ with $f_x = 0.0075\ \epsilon\sigma^{-1}$, $\epsilon_{wf} = 0.2\epsilon$.

In the employed model the wall particles are allowed to vibrate around their crystalline sites based on a spring potential. Consequently, due to the absence of interatomic interactions, there is no solid elasticity in the wall and, therefore, this model tends to neglect the molecular diffusion. Despite the absence of solid elasticity (frequently neglected in molecular studies [24,25]), the thermal vibrations of the wall particles are simulated effectively. Although this type of thermal walls is expected to provide slightly overestimated figures for the slip, due to the absence of solid elasticity, it is a widely adopted approach in the literature [9,20,21]. In more sophisticated models, where the wall particles are not anchored to their lattice sites, the presence of interatomic interactions and molecular diffusion in the wall alters the original structure of the lattice and, therefore, additional nanoscale roughness is introduced affecting the frictional coefficient. Results from previous MD studies show small variations between models with and without solid elasticity [9,26,27].

III. RESULTS AND DISCUSSION

Figure 1 shows examples of averaged fluid density profiles under different values of surface stiffness. These simulations have been carried out with interaction parameters $\epsilon_{wf} = 0.2\epsilon$, $\sigma_{wf} = 0.75\sigma$ and an external driving force $f_x = 0.0075\ \epsilon\sigma^{-1}$. A common element observed in the density distributions is their profound oscillations near the solid wall. Despite the changes in the surface stiffness, the density follows the same pattern, since the locations of its local maxima and minima remain almost constant and rests to its bulk value after $(5-7)\sigma$. The variation of the spring stiffness primarily influences the density absolute maximum value and for the simulations considered in Fig. 1 this value increases, with a nonlinear manner, as κ increases from $\kappa = 100\ \epsilon\sigma^{-2}$ to $\kappa = 600\ \epsilon\sigma^{-2}$. Furthermore, deviations between the results are reduced as higher surface stiffness rates are employed in the numerical simulations (see Fig. 1). Smaller κ implies that the wall particles oscillate around their equilibrium positions with higher amplitude and lower frequency and therefore the fluid molecules can potentially travel closer to the solid wall

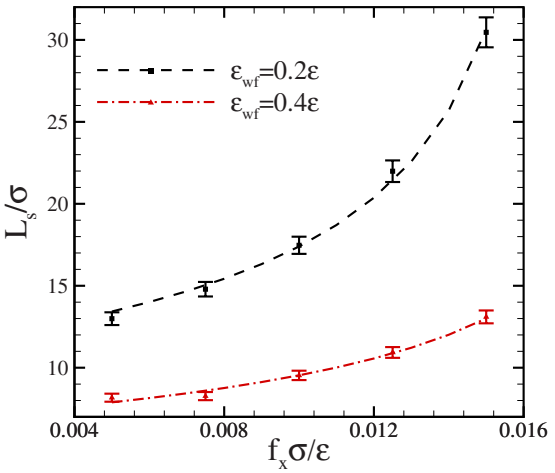

FIG. 2. (Color online) Slip length variations with length L_s as a function of the driving force f_x for wall particles with stiffness $\kappa = 900\ \epsilon\sigma^{-2}$; the dashed curves are the best fitting to $L_s(f_x)=L_s^0(1-f_x/f_c)^{-0.5}$.

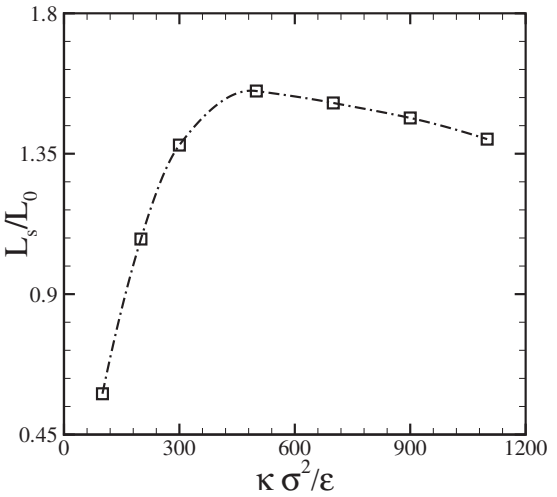

FIG. 3. Variation of the slip length as a function of surface stiffness for a flow with $f_x=0.01\ \epsilon\sigma^{-1}$, $\epsilon_{wf}=0.4\epsilon$.

[9]. As a consequence, a broader density profile is observed near the first peak. However, as the spring stiffness κ increases its influence on the wall particles oscillations is primarily related to oscillation frequency rather than oscillation amplitude, which is mainly determined by the wall temperature [23]. Thus, its impact on the in-plane fluid layering and hence on the density profile is less apparent.

Figure 2 shows the variation of the slip length for a certain value of stiffness $\kappa=900\ \epsilon\sigma^{-2}$ as a function of the driving force f_x. Previous MD studies [7,9] report that the slip length variations are well described by a power law function

$$L_s(f_x) = L_s^0(1 - f_x/f_c)^{-0.5}, \tag{5}$$

where L_s^0 represents an asymptotical value of the slip length as the shear rate tends to zero and f_c corresponds to a critical driving force value. As the driving force approaches this critical value f_c, the slip length appears to diverge [7]. In Fig. 2 the computational uncertainty in the slip length calculations is approximately 3%. The simulation data were fitted through Eq. (5) and the obtained parameters for $\epsilon_{wf}=0.2\epsilon$ and $\epsilon_{wf}=0.4\epsilon$ are $L_s^0=11.33\sigma$, $f_c=0.0174\ \epsilon\sigma^{-1}$, and $L_s^0=6.88\sigma$, $f_c=0.021\ \epsilon\sigma^{-1}$, respectively. The calculated slip lengths (Fig. 2) are in good agreement with analytical results derived by previous studies [7,9]. The change rate of the slip length increases as the driving force moves toward to its critical value.

Figure 3 shows an example of the slip length as a function of surface stiffness. In the performed molecular simulations the interaction parameters are $\epsilon_{wf}=0.4\epsilon$, $\sigma_{wf}=0.75\sigma$ and the external driving force is $f_x=0.01\ \epsilon\sigma^{-1}$. In Fig. 3 the slip length has been scaled with L_0, which represents the slip length when a fixed lattice wall is employed. In this wall model the solid particles are immobilized in their lattice sites and, therefore, are not allowed to vibrate [7,23]. Figure 3 shows that the slip varies along with the surface stiffness. For the less stiff surfaces, such as for $\kappa=100\ \epsilon\sigma^{-2}$ (Fig. 3), the effect of slip is smaller than the one calculated when a fixed lattice wall is employed. Smaller values of κ imply larger displacements of the wall particles resulting to an increased surface roughness. In this case, the interactions between the wall and fluid particles lead to improved momentum transfer and, consequently, to less slippage. As κ increases, the surface of the wall becomes effectively smoother and higher slip is produced. However, Fig. 3 shows that instead of the slip length increasing monotonically with the wall stiffness, it obtains a maximum value $L_{s,max}$ and then starts to reduce. When stiffer walls are employed the impact of bonding stiffness on the oscillation amplitude of the wall particles is continuously decreasing. The amplitude, as already mentioned, is primarily dictated by the temperature of the walls and, therefore, κ is no longer a dominant factor for the surface smoothness or roughness. Therefore, increasing the values of κ alters the oscillation frequency toward higher values that contribute to a more efficient interfacial momentum transfer and, consequently, to a reduction in the slip length. This is justified for values of stiffness κ that lead to oscillating periods T_{oscill} higher than the mean molecular collision time (τ_{coll}); in the present study this is valid for $\kappa < 2000\ \epsilon\sigma^{-2}$.

The relative growth and decay of the mean frequency and amplitude as a function of κ are shown in Fig. 4. These variations are calculated as $(f_\kappa - f_{\kappa=100})/f_{\kappa=100}$ and $(d_{\kappa=100} - d_\kappa)/d_{\kappa=100}$, where f corresponds to the mean oscillating frequency and d to the mean vibrating amplitude of the wall particles. The values for $\kappa=100\ \epsilon\sigma^{-2}$ are $f_{\kappa=100}=1.6721/\tau$ corresponding to a mean oscillation time $T_{oscill,\kappa=100}=0.598\tau$ and $d_{\kappa=100}=5.3\times10^{-4}\sigma$. Figure 4 shows that for higher stiffness values there is almost a linear increase for the frequency with the decay rate of the mean displacement approaching zero.

Similar behavior has been observed in all the performed simulations regardless the various wall-fluid interactions or shear rates employed. The results of the numerical experiments are summarized in Fig. 5. Here, the slip length has been scaled with $L_{s,max}$, which represents its maximum value in a series of simulations with the same interaction parameters, driving force and variable κ. The stiffness has been

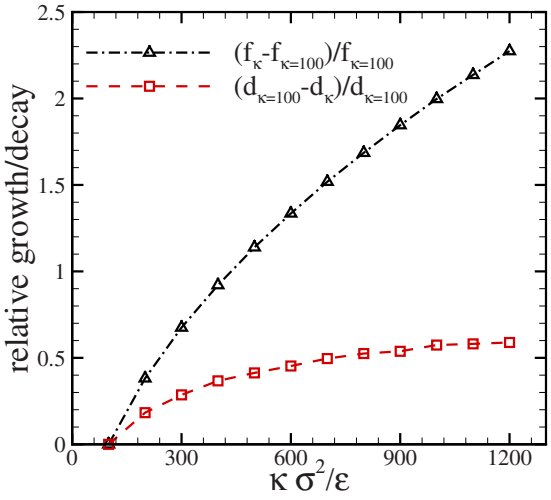

FIG. 4. (Color online) Relative variations of the mean oscillation amplitude and frequency (with respect to mean amplitude and frequency for $\kappa=100$) as a function of stiffness κ.

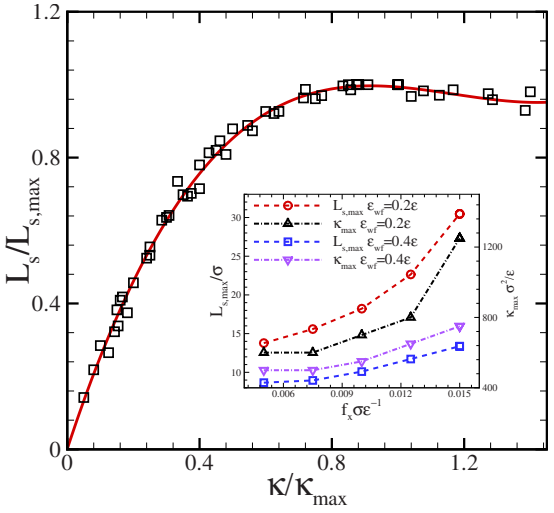

FIG. 5. (Color online) "Master" curve describing the variation of the slip length as a function of wall stiffness. The inset shows how the values $L_{s,max}$ and κ_{max} vary with the driving force f_x for different interaction parameters.

scaled with κ_{max}, which represents the value of κ that maximizes the slip. It is apparent that the parameters $L_{s,max}$ and κ_{max} depend on the various simulations conditions such as shear rate or surface attraction energy. Figure 5 shows that the effect of the wall stiffness on the slip process can be well quantified by a "master" curve, which in our case is a fifth-order polynomial

$$\frac{L_S}{L_{S,max}} = a + b\frac{\kappa}{\kappa_{max}} + \cdots + f\left(\frac{\kappa}{\kappa_{max}}\right)^5 \tag{6}$$

where $a=0.01$, $b=2.59$, $c=-1.68$, $d=-0.77$, $e=1.16$, and $f=-0.32$. In addition, Fig. 5 suggests that the selection of the wall stiffness during the molecular simulations should be carefully selected since it can lead to various slip scenarios. Potentially, the "master" curve can be extended to accommodate the variation of $L_{s,max}$ and κ_{max} as function of other parameters that are important to the slip process, like for example the shear rate.

IV. CONCLUDING OVERVIEW

An investigation of the relationship between the wall stiffness and the slip produced was carried out. We show that the slip length variations as a function of surface stiffness can be approximated and well described through a master curve. Quantifying the dependence of L_s on κ provides a mechanism for obtaining a better insight in the slip phenomena and reducing the variability regarding the values of surface stiffness employed in molecular simulations. Generally, the stiffness factor influences not only the slip process but also the thermal equilibrium at the solid liquid interface [23]. Further studies toward a better understanding of the stiffness effects on the slip and thermal transfer phenomena are also currently being pursued. Specifically, the combined effects of the mass of the wall particles mass and the surface stiffness are studied along with more realistic models for the thermal walls.

[1] C. Choi, K. Westin, and K. Breuer, Phys. Fluids **15**, 2897 (2003).
[2] D. C. Tretheway and C. D. Meinhart, Phys. Fluids **14**, L9 (2002).
[3] Y. Zhu and S. Granick, Phys. Rev. Lett. **88**, 106102 (2002).
[4] M. Sbragaglia, R. Benzi, L. Biferale, S. Succi, and F. Toschi, Phys. Rev. Lett. **97**, 204503 (2006).
[5] N. V. Priezjev, A. A. Darhuber, and S. M. Troian, Phys. Rev. E **71**, 041608 (2005).
[6] C. Cottin-Bizonne, J.-L. Barrat, L. Bocquet, and E. Charlaix, Nature Mater. **2**, 237 (2003).
[7] P. A. Thompson and S. M. Troian, Nature (London) **389**, 360 (1997).
[8] J. L. Barrat and L. Bocquet, Phys. Rev. Lett. **82**, 4671 (1999).
[9] N. V. Priezjev, J. Chem. Phys. **127**, 144708 (2007).
[10] C. Cottin-Bizonne, C. Barentin, E. Charlaix, L. Bocquet, and J.-L. Barrat, Eur. Phys. J. C **15**, 427 (2004).
[11] E. Bonaccurso, H.-J. Butt, and V. S. J. Craig, Phys. Rev. Lett. **90**, 144501 (2003).
[12] T. M. Galea and P. Attard, Langmuir **20**, 3477 (2004).
[13] N. V. Priezjev and S. M. Troian, J. Fluid Mech. **554**, 25 (2006).
[14] F. D. Sofos, T. E. Karakasidis, and A. Liakopoulos, Phys. Rev. E **79**, 026305 (2009).
[15] Y. Zhu and S. Granick, Phys. Rev. Lett. **87**, 096105 (2001).
[16] K. Binder, J. Horbach, W. Kob, P. Wolfgang, and V. Fathollah, J. Phys. Condens. Matter **16**, S429 (2004).
[17] G. S. Grest and K. Kremer, Phys. Rev. A **33**, 3628 (1986).
[18] M. P. Allen and D. J. Tildesley, *Computer Simulation of liquids* (Oxford University Press, Oxford, 1987).

[19] J. L. Barrat and J. P. Hansen, *Basic Concepts for Simple and Complex liquids* (Oxford University Press, Oxford, 2003).
[20] A. Jabbarzadeh, J. D. Atkinson, and R. I. Tanner, J. Chem. Phys. **110**, 2612 (1999).
[21] M. Cieplak, J. Koplik, and J. R. Banavar, Phys. Rev. Lett. **86**, 803 (2001).
[22] K. Petersen, IEEE Trans. Electron Devices **25**, 1241 (1978).
[23] B. H. Kim, A. Beskok, and T. Cagin, Microfluid. Nanofluid. **5**, 551 (2008).
[24] J. Koplik, J. R. Banavar, and J. F. Willemsen, Phys. Fluids A **1**, 781 (1989).
[25] P. A. Thompson and M. O. Robbins, Phys. Rev. A **41**, 6830 (1990).
[26] P. Yi, D. Poulikakos, J. Walther, and G. Yadigaroglu, Int. J. Heat Mass Transfer **45**, 2087 (2002).
[27] R. Branam and M. M. Micci, Nanoscale Microscale Thermophys. Eng. **13**, 1 (2009).